Math. Struct. in Comp. Science (2007), *vol.* 17, *pp.* 1117–1132.
doi:10.1017/S0960129507006329 Printed in the United Kingdom

Entanglement and Hilbert space geometry for systems with a few qubits

REMY MOSSERI and PEDRO RIBEIRO

Laboratoire de Physique Théorique de la Matire Condense, CNRS UMR 7600,
Université Pierre et Marie Curie Paris 6, Tour 24, Boite 121,
4 place Jussieu, 75252 Paris Cedex 05 France
Email: mosseri@ccr.jussieu.fr; pedro@lptmc.jussieu.fr

Received 24 November 2006

This paper reviews recent attempts to describe the two- and three-qubit Hilbert space geometries. In the first part, this is done with the help of Hopf fibrations of hyperspheres. It is shown that the associated Hopf map is strongly sensitive to states' entanglement content. In the two-qubit case, a generalisation of the celebrated one-qubit Bloch sphere representation is described. In the second part, we present Hilbert space discrete versions, which are comparable to polyhedral approximations of spheres in standard geometry.

1. Introduction

The rapidly growing field of quantum information is based on the subtle and often counter-intuitive properties of quantum-state entanglement (Bouwmeester *et al.* 2000; Nielsen and Chuang 2000). It is therefore of great interest to have a geometrical picture of this latter property, directly written in the Hilbert space where the quantum evolution takes place. However, even with a few qubits, this space is of high dimension, which makes it difficult to visualise, and entanglement turns out to be a complicated concept (see, for example, Kus and Zyczkowski (2001) and Levay (2004)).

In this paper, we show that this task can, nevertheless, be accomplished fully for two qubits, and partly for three qubits. For one qubit (a single two-level system), a well-known tool in quantum optics is the Bloch sphere (S^2) representation, which is related to Hopf fibration of the S^3 hypersphere (Urbanke 1991). A generalisation for a two-qubit system has been proposed (Mosseri and Dandoloff 2001) in the framework of the S^7 sphere Hopf fibration, and will be recalled below. An interesting result is that the S^7 Hopf fibration is entanglement sensitive, and therefore provides a kind of foliation for the 2 qubits (projective) Hilbert space with respect to their entanglement content. An extension of this description to a three-qubit system, using the S^{15} Hopf fibration, will also be presented here.

In the second part of the paper we present some optimal discretised Hilbert spaces (which are similar to what polytopes are to continuous hyperspheres), and their interesting relation to dense sphere packings in high-dimensional real space.

2. Entanglement and Hopf fibrations

An n-qubit state can be written as

$$|\Psi\rangle = \sum_{l=0}^{2^n-1} t_l\,|l\rangle \quad \text{with} \quad t_l \in \mathbb{C}, \text{ and the normalisation } \sum |t_l|^2 = 1\,.$$

Here $|l\rangle$ stands for the n-qubit base-2 decomposition of the integer l, with each qubit being associated with one basis factor of the n-qubit tensor product

$$|l\rangle = |\alpha_1\rangle_1 \otimes |\alpha_2\rangle_2 \otimes \cdots |\alpha_n\rangle_n$$

where $\alpha_j = 0$ or 1 according to the decomposition of l. In principle, the n-qubit Hilbert space is $\mathbb{C}^{2^n}$, or $\mathbb{C}P^{2^n-1}$ for the projective version where the global phase freedom is taken into account. But the normalisation condition makes it more natural to consider $S^{2^{n+1}-1}$ spheres embedded in $\mathbb{R}^{2^{n+1}}$.

2.1. *One qubit, Bloch sphere and the S^3 Hopf fibration*

A single qubit state can be written as

$$|\Psi\rangle = t_0\,|0\rangle + t_1\,|1\rangle\,, \qquad t_0, t_1 \in \mathbb{C}, |t_0|^2 + |t_1|^2 = 1\,. \tag{1}$$

Viewed as pairs of real numbers, the two normalised components t_0, t_1 generate a unit radius sphere S^3 embedded in $\mathbf{R}^4$. The global phase freedom sends the S^3 sphere to the (unit radius) S^2 Bloch sphere, with coordinates related to expectation values of the standard spin operators (represented by the Pauli matrices).

To describe the Hopf map in an analytical form, we go back to the definition of S^3 as pairs of complex numbers (t_0, t_1). The Hopf map is defined as the composition of a map h_1 from S^3 to R^2 $(+\infty)$, followed by an inverse stereographic map h_2 from R^2 to S^2:

$$h_1 : \begin{array}{ccc} S^3 & \longrightarrow & R^2 + \{\infty\} \\ (t_0, t_1) & \longrightarrow & C = \overline{t_0 t_1^{-1}} \end{array} \qquad t_0, t_1 \in \mathbb{C}$$

$$h_2 : \begin{array}{ccc} R^2 + \{\infty\} & \longrightarrow & S^2 \\ C & \longrightarrow & M(X, Y, Z) \end{array} \qquad X^2 + Y^2 + Z^2 = 1 \tag{2}$$

where $\overline{z}$ is the complex conjugate of z. The first map h_1 clearly shows that the full S^3 great circle, parametrised by $(t_0 \exp i\omega, t_1 \exp i\omega)$, is mapped onto the same single point with complex coordinate C. It is easy to show that, with R^2 cutting the unit radius S^2 along the equator, and the north pole (along the Z axis) as the stereographic projection pole, the S^2 Hopf fibration base coordinates coincide with the well-known S^2 Bloch sphere coordinates:

$$\begin{aligned} X &= \langle \sigma_x \rangle_\Psi = 2\,\mathrm{Re}(\overline{t_0} t_1) \\ Y &= \langle \sigma_y \rangle_\Psi = 2\,\mathrm{Im}(\overline{t_0} t_1) \\ Z &= \langle \sigma_z \rangle_\Psi = |t_0|^2 - |t_1|^2\,. \end{aligned}$$

https://doi.org/10.1017/S0960129507006329 Published online by Cambridge University Press

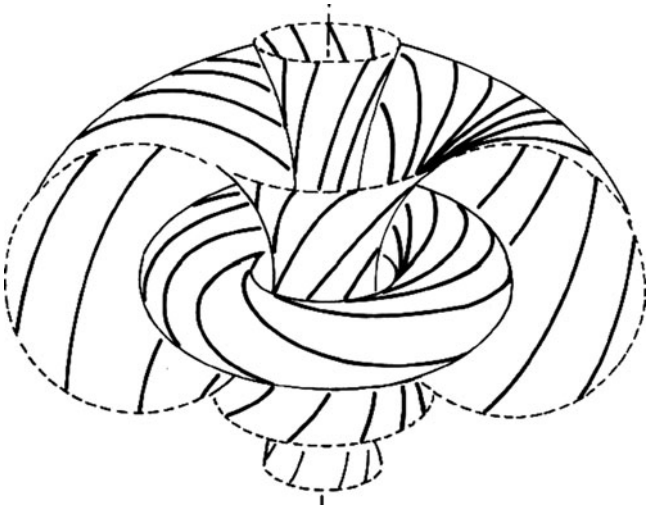

Fig. 1. S^3 Hopf fibration after a stereographic map onto R^3. Circular S^1 fibres are mapped onto circles in R^3, apart from the exceptional fibre through the projection pole, which is mapped onto a vertical straight line. Fibres can be grouped into a continuous family of nested tori, three of which are shown in the figure.

The $\sigma_{x,y,z}$ are the standard Pauli matrices (we add the identity matrix as the matrix σ_w for later use):

$$\sigma_w = \begin{bmatrix} 1 & 0 \\ 0 & 1 \end{bmatrix} \quad \sigma_z = \begin{bmatrix} 1 & 0 \\ 0 & -1 \end{bmatrix}$$

$$\sigma_x = \begin{bmatrix} 0 & 1 \\ 1 & 0 \end{bmatrix} \quad \sigma_y = \begin{bmatrix} 0 & -i \\ i & 0 \end{bmatrix}.$$

It is tempting to try to visualise the full (S^3) Hilbert space with its fibre structure. This can be achieved through a (direct) stereographic map from S^3 to R^3 (Figure 1). Each S^3 circular fibre is mapped onto a circle in R^3, apart from the image of the unique S^3 great circle passing through the projection pole, which is a straight line.

One way to obtain a global phase free description is to use the density matrix description, which reads for this pure case as the projector

$$\rho_\Psi = |\Psi\rangle \langle\Psi| = \frac{1}{2} \begin{pmatrix} 1+Z & X-iY \\ X+iY & 1-Z \end{pmatrix}.$$

It is clear that $\rho_\Psi = \rho_{e^{i\varphi}\Psi}$, for any angle φ, which shows that the pure state density matrix represents the quantum phase up to a global phase. The vanishing determinant of ρ is related to the unit radius of the Bloch sphere. For one-qubit mixed states, the latter condition is relaxed and density matrices are represented by points inside a unit ball B^3 limited by the Bloch sphere.

https://doi.org/10.1017/S0960129507006329 Published online by Cambridge University Press

2.2. *Two-qubit entanglement and the S^7 Hopf fibration*

A generic two-qubit state can be written as

$$|\Psi\rangle = t_0\,|00\rangle + t_1\,|01\rangle + t_2\,|10\rangle + t_3\,|11\rangle$$

where we have explicitly used the base-2 decomposition to highlight the underlying tensor product. A state $|\Psi\rangle$ is said to be 'separable' if, through the use of individual qubit basis rotations, it can be written as a simple product:

$$|\Psi\rangle = |\varphi\rangle_1 \otimes |\theta\rangle_2 .$$

It is easy to show that this is only possible if

$$t_0 t_3 - t_1 t_2 = 0 .$$

The deviation of the left-hand side from zero leads to a measure of state entanglement

$$c = 2\,|t_0 t_3 - t_1 t_2| ,$$

which is known as the 'concurrence' (Wootters 1998), which will play an important role below. Indeed, we aim to foliate the two qubit projective Hilbert space $\mathbb{C}P^3$, in terms of equi-concurrence manifolds. As will soon become clear, the S^7 Hopf fibration will prove to be of great help in fulfilling this task (Mosseri and Dandoloff 2001).

The S^7 Hopf fibration is defined along the same lines as in the S^3 case, but using quaternions (with the quaternion algebra denoted $\mathbb{Q}$), instead of complex numbers. We combine two complex components into a quaternion (using the quaternionic $\mathbf{j}$ unit) in the form

$$q_1 = t_0 + t_1\mathbf{j},\ q_2 = t_2 + t_3\mathbf{j}, \qquad q_{1,}q_2 \in \mathbb{Q} . \tag{3}$$

A point (representing the state $|\Psi\rangle$) on the unit radius S^7 is represented as a pair of quaternions $(q_{1,}q_2)$ satisfying $|q_1|^2 + |q_2|^2 = 1$. The Hopf map from S^7 to the base S^4 is the composition of a map h_1 from S^7 to R^4 $(+\infty)$, followed by an inverse stereographic map h_2 from R^4 to S^4.

$$h_1 : \begin{array}{ccc} S^7 & \longrightarrow & R^4 + \{\infty\} \\ (q_1, q_2) & \longrightarrow & Q = \overline{q_1 q_2^{-1}} \end{array} \qquad q_{1,}q_2 \in \mathbb{Q}$$

$$h_2 : \begin{array}{ccc} R^4 + \{\infty\} & \longrightarrow & S^4 \\ Q & \longrightarrow & M(x_l) \end{array} \qquad \sum_{l=0}^{l=4} x_l^2 = 1 . \tag{4}$$

The base space S^4 is not embedded in S^7: the fibration is again non-trivial (as in the S^3 case). The fibre is a unit S^3 sphere: the S^7 points $(q_{1,}q_2)$ and $(q_1 q, q_2 q)$, with q a unit quaternion (geometrically an S^3sphere) are mapped onto the same Q value.

Writing Q in terms of the original components t_l,

$$Q = \overline{q_1 q_2^{-1}} = \frac{1}{\sin^2(\theta/2)}\,(C_1 + C_2\mathbf{j}) \tag{5}$$

with $\sin(\theta/2) = |q_2|$, $C_1 = \left(\overline{t_0}t_2 + \overline{t_1}t_3\right)$, $C_2 = (t_0 t_3 - t_1 t_2)$ and $C_1, C_2 \in \mathbb{C}$.

https://doi.org/10.1017/S0960129507006329 Published online by Cambridge University Press

The simple relation between the concurrence entanglement measure c and the C_2 term is striking: $c = 2|C_2|$. This shows that, if correctly oriented, *the Hopf map is entanglement sensitive*! Indeed, states that are mapped onto pure complex values for Q are separable states. In addition, the fibre structure implies that a whole S^3 manifold is singled out with the same entanglement content.

It is also instructive to consider the S^4 base coordinates,

$$\begin{aligned} x_0 &= |q_1|^2 - |q_2|^2 \\ &= \langle \sigma_z \otimes Id \rangle_\Psi \\ x_1 + \mathbf{i}x_2 &= 2\left(\overline{t_0}t_2 + \overline{t_1}t_3\right) \\ &= \langle (\sigma_x + i\sigma_y) \otimes Id \rangle_\Psi \\ x_3 + \mathbf{i}x_4 &= 2\left(t_0 t_3 - t_1 t_2\right). \end{aligned} \tag{6}$$

We can now foliate $\mathbb{C}P^3$ with respect to c. Recall that one must identify states that are equivalent under a global phase shift: $e^{i\varphi}|\Psi\rangle \sim |\Psi\rangle$. Under multiplication by $e^{i\varphi}$, the first three coordinates on the base S^4 are left unchanged, while $x_3 + ix_4$ suffers a doubled phase shift $e^{2i\varphi}$. Apart from $c = 0$ (separable states), this implies that for fixed c the projective manifold is generically the product of a partial Bloch sphere and an S^3 sphere with opposite points identified, which corresponds to an $SO(3)$ manifold. When $c = 0$, the situation is different since multiplying Ψ by $e^{i\varphi}$ precisely moves the representative point onto a circle of the Hopf fibration on the S^3 fibre (the latter then reduces to the partial Bloch sphere of the second qubit). So, for separable two-qubit states, one recovers the expected result that the projective Hilbert space is the product of the two partial Bloch spheres. In all cases, the partial Bloch sphere radius r is simply related to the concurrence through $r = \sqrt{1 - c^2}$. One also recovers the fact that this radius vanishes for maximally entangled states (MES), and the MES manifold reduces to $SO(3)$.

Note also that any MES can be obtained from a separable 2-qubit state under the action of an (antilinear) operator

$$K = \frac{1}{\sqrt{2}}(1 + T)$$

with T the time-reversal operator $T = -J(\sigma_y \otimes \sigma_y)$, and J the operator (acting here on the left) that takes the complex conjugate of all complex numbers involved in an expression. This correspondance is many-to-one since the MES manifold ($SO(3)$) is 3 dimensional, while the separable manifold ($S^2 \times S^2$) is 4 dimensional

As a whole, the concurrence based foliation of $\mathbb{C}P^3$, with $r = \sqrt{1 - c^2}$, is given by Figure 2.

2.3. *Three qubits and the S^{15} Hopf fibration*

A generic three-qubit state can be written as

$$|\Psi\rangle = \sum_{l=0}^{7} t_l |l\rangle \quad \text{with} \quad t_l \in \mathbb{C}, \text{ and } \sum |t_l|^2 = 1.$$

https://doi.org/10.1017/S0960129507006329 Published online by Cambridge University Press

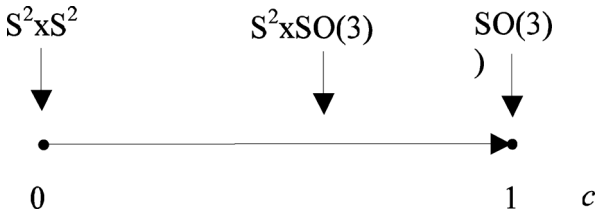

Fig. 2. Foliation of the two-qubit Hilbert space with respect to state entanglement.

The $|\Psi\rangle$ normalisation condition leads us to consider the 15-dimensional sphere S^{15} embedded in R^{16}. This suggests looking to see whether the third Hopf fibration (that of S^{15}, with base S^8 and fibres S^7) could be helpful in describing the three-qubit Hilbert space geometry (Bernevig and Chen 2003; Mosseri 2006). One should first recognise that the concept of entanglement becomes more complicated as more qubits are added. Should we consider the entanglement of one qubit with respect to the other two qubits (irrespective of the degree of entanglement between these latter two), or some 'true' three-qubit entanglement, as measured for instance by the 3-tangle (Coffman *et al.* 2000)?

It is interesting here to recall the notion of entanglement invariants, which are functions of the state component t_l and are invariant under the action of local unitary operations (the latter leaving entanglement unchanged). For two qubits, there are 2 such invariants, the (trivial) norm of the state and the concurrence. As we have seen, the latter can also be expressed in term of the partial Bloch sphere radius ($r = \sqrt{1-c^2}$), which is the same for the two qubits. Therefore, as shown above, the S^7 Hopf map displays the two-qubit invariant. For three qubits, there are 6 invariants, which can be expressed in different ways. A possible choice is the norm of the state, the three radii r_j, $j = 1 \cdots 3$ of the partial Bloch spheres, the 3-tangle τ_3 together with one more that was introduced by J. Kempe (Kempe 1999)

Omitting the trivial norm invariant, we would like to foliate the (14-dimensional) three-qubit projective Hilbert space $\mathbb{C}P^7$ with respect to the different values of the invariant 5-tuplets. This task is rather complicated, and has not yet been fully completed; however, we shall see now that the S^{15} Hopf fibrations can tell us something about this manifold.

To define the fibration, one proceeds along the same lines as for the previous S^3 and S^7 cases, but now using octonions (with the octonion algebra denoted $\mathbb{O}$). The interested reader should refer to the appendix of Mosseri (2006) for information about the octonion multiplication that is used here. We write

$$a = a' + a''\mathbf{e},\ b = b' + b''\mathbf{e}, \qquad a, b \in \mathbb{O}, \text{ and } a', a'', b', b'' \in \mathbb{Q}, \tag{7}$$

and a point (representing the state $|\Psi\rangle$) on the unit radius S^{15} as a pair of octonions (a, b) satisfying $|a|^2 + |b|^2 = 1$. But, to get a Hopf map of physical interest, with coordinates simply related to interesting observable expectation values, one needs to define a slightly tricky relation between $|\Psi\rangle$ and the pair of octonions (a, b) as follows:

$$\begin{aligned} a &= (t_0 + t_1\mathbf{j}, t_2 + \mathbf{j}t_3) = (t_0 + t_1\mathbf{j}, t_2 + \overline{t_3}\mathbf{j}) = \left(a', a''\right) \\ b &= (t_4 + t_5\mathbf{j}, t_6 + \mathbf{j}t_7) = (t_4 + t_5\mathbf{j}, t_6 + \overline{t_7}\mathbf{j}) = \left(b', b''\right). \end{aligned} \tag{8}$$

https://doi.org/10.1017/S0960129507006329 Published online by Cambridge University Press

The Hopf map from S^{15} to the base S^8 is the composition of a map h_1 from S^{15} to R^8 $(+\infty)$, followed by an inverse stereographic map h_2 from R^8 to S^8:

$$h_1 : \begin{array}{ccc} S^{15} & \longrightarrow & R^8 + \{\infty\} \\ (a,b) & \longrightarrow & P = \overline{ab^{-1}} \end{array} \qquad a, b \in \mathbb{O}$$

$$h_2 : \begin{array}{ccc} R^8 + \{\infty\} & \longrightarrow & S^8 \\ P & \longrightarrow & M(x_l) \end{array} \qquad \sum_{l=0}^{l=8} x_l^2 = 1\,. \tag{9}$$

The base space S^8 is not embedded in S^{15}: the fibration is again non-trivial. The fibre is a unit S^7 sphere, the proof of which is trickier (and not given here) than in the lower dimension case. The h_1 map leads to

$$P = \overline{ab^{-1}} = \frac{1}{\sin^2\theta/2}\,(Q_1 + Q_2\mathbf{e}) \tag{10}$$

with $\sin\theta/2 = |b|$, $Q_1 = (b'\overline{a'} + \overline{a''}b'')$, $Q_2 = \left(-a''b' + b''a'\right)$ and $Q_1, Q_2 \in \mathbb{Q}$.

Athough it is not evident at first sight, the Hopf map is still entanglement sensitive in this case. To show this, it is instructive first to express Q_1 and Q_2 in terms of the t_l components read out from (8):

$$Q_1 = \left(\overline{t_0}t_4 + \overline{t_1}t_5 + \overline{t_2}t_6 + \overline{t_3}t_7\right) + \left(t_0t_5 - t_1t_4 + \overline{t_2t_7} - \overline{t_3t_6}\right)\,\mathbf{j}$$

$$Q_2 = \left(t_0t_6 + t_2t_4 + \overline{t_3t_5} - \overline{t_1t_7}\right) + \left(t_1t_6 - t_2t_5 + \overline{t_0t_7} - \overline{t_3t_4}\right)\,\mathbf{j}\,.$$

Introducing the generalised complex concurrence terms $T_{ij,kl} = t_it_j - t_kt_l$ allows us to write the coordinates on the unit radius base S^8 in a synthetic form. The second map h_2 sends states onto points on S^8, with coordinates x_l, with l running from to 0 to 8. With the inverse stereographic pole located on the S^8 'north pole' ($x_0 = +1$), and the target space R^8 cutting S^8 along the equator, we get the following coordinate expressions

$$\begin{aligned} x_0 &= \cos\theta \\ &= |a|^2 - |b|^2 \\ &= \langle \sigma_z \otimes Id \otimes Id \rangle_\Psi \\ x_1 + \mathbf{i}\,x_2 &= 2\left(\overline{t_0}t_4 + \overline{t_1}t_5 + \overline{t_2}t_6 + \overline{t_3}t_7\right) \\ &= \left\langle \left(\sigma_x + \mathbf{i}\,\sigma_y\right)_1 \otimes Id \otimes Id \right\rangle_\Psi \\ x_3 + \mathbf{i}\,x_4 &= 2\left(T_{05,14} + \overline{T_{27,36}}\right) \\ x_5 + \mathbf{i}\,x_6 &= 2\left(T_{06,24} + \overline{T_{35,17}}\right) \\ x_7 + \mathbf{i}\,x_8 &= 2\left(T_{16,25} + \overline{T_{07,34}}\right)\,. \end{aligned} \tag{11}$$

Three-qubit states in which the first qubit is separated from the other two map onto a point such that $x_j = 0$, for $j = 3 \cdots 8$. Indeed, in a multi-qubit state, a given qubit is separated from the others when its partial Bloch sphere has a radius $r_1 = 1$. The first qubit partial Bloch sphere is spanned here by the triplet (x_0, x_1, x_2). Returning to the above definition of the h_1 map, this means that in that case the Hopf map carries an

https://doi.org/10.1017/S0960129507006329 Published online by Cambridge University Press

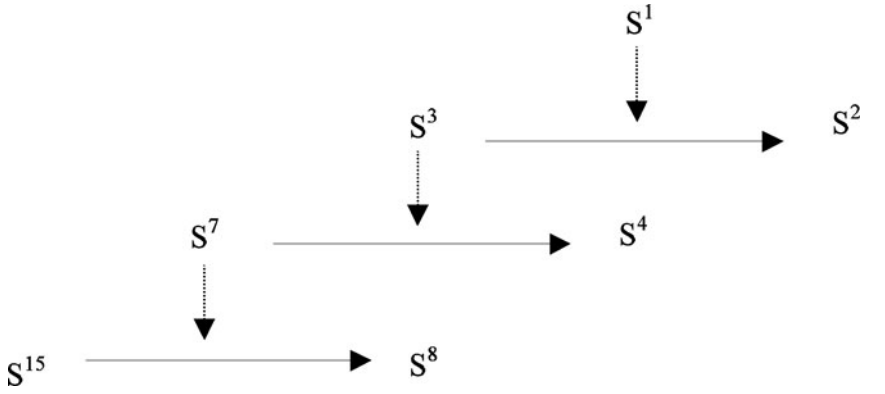

Fig. 3. Nesting of the three Hopf fibrations.

octonion couple onto a pure complex number P. Therefore, as for the two-qubit case, *the S^{15} Hopf fibration is also entanglement sensitive for three qubits!*

After modding out the global phase (we aim to describe the projective Hilbert space $\mathbb{C}P^7$), the first three base coordinates remain invariant. When $r_1 < 1$, multiplication of $|\Psi\rangle$ by $e^{i\varphi}$ induces a complex orbit of the representative point spanned by the six coordinates $x_{3\cdots 8}$, which live on an S^5 sphere of radius $r_1' = \sqrt{1 - r_1^2}$. We call $M(r_1')$, without further characterisation, the manifold obtained as the S^5 sphere modulo these orbits. In addition, when $\varphi = \pi$ the representative point returns to its original position on the base. This means that a given S^7 fibre appears twice along this orbit, opposite points being identified. The S^7 fibre is then turned into a 7-dimensonal real projective plane $\mathbb{R}P^7$. We eventually get the following foliation of $\mathbb{C}P^7$ with respect to the single invariant r_1:

— For $r_1 = 1$, it is the product of radius one sphere S^2 (which is also $\mathbb{C}P^1$), with $\mathbb{C}P^3$, the projective Hilbert space of the second and third qubit. Note that, here, multiplication by a complex number leaves the S^7 fibre invariant, and, therefore, modding out the base sends it to $\mathbb{C}P^3$.

— For $0 < r_1 < 1$, it is the product of $S^2(r_1)$ (a sphere of radius r_1), the $M(r_1')$ manifold and $\mathbb{R}P^7$

— For $r_1 = 0$, it is the product of the $M(1)$ manifold and $\mathbb{R}P^7$

Note that there is nothing special about the first qubit, apart from a special orientation of the Hopf fibration that singles out its properties. A better insight into an entanglement-based foliation problem would be to use three distinct S^{15} Hopf fibrations (instead of one), such that each of the three qubit partial Bloch spheres is singled out by the first three coordinates on the base. Put more simply, one may try to describe the Hilbert space geometry in a space spanned by the three partial Bloch sphere radii (r_1, r_2, r_3). But this is not the end of the story, since there will still be two other invariants to take into account.

Finally, let us stress the nice nesting of the three Hopf fibrations of S^3, S^7 and S^{15}, the fibre in the larger dimensional space being the the full fibred space in the lower dimensional case, as illustrated in Figure 3.

https://doi.org/10.1017/S0960129507006329 Published online by Cambridge University Press

3. Hilbertian polytopes

In this section, we describe discretised versions of the n-qubit projective Hilbert space $\mathbb{C}P^{2^n-1}$, which are analogous to standard polytopes with respect to spherical spaces. These 'Hilbertian polytopes' will be described using two *a priori* different (algebraic and geometric) approaches, which eventually lead to the same structures. These structures have been defined from a generic point of view, and details given for one and two qubits by C. Rigetti, M. Devoret and one of the current authors (Remy Mosseri) in Rigetti *et al.* (2004). This construction will be recalled briefly here; in addition, we will also describe the three-qubit case, with its 1080 states in $\mathbb{C}P^7$.

3.1. *Discretisation based on stabiliser theory*

We first define the n-qubit Pauli group $\mathscr{G}_n$ as the set of all n-fold tensor products of 2×2 Pauli matrices, with four possible overall phases to satisfy the closure requirement:

$$\mathscr{G}_n = \{\sigma_w, \sigma_x, \sigma_y, \sigma_z\}^{\otimes n} \otimes \{\pm 1, \pm i\} \ .$$

We use $\Sigma_{\alpha\beta\ldots\zeta} = \sigma_\alpha \otimes \sigma_\beta \otimes \cdots \otimes \sigma_\zeta$ to denote the generalised Pauli matrices.

Here we disregard the phases $\{\pm 1, \pm i\}$ required for closure of $\mathscr{G}_n$ under multiplication and deal with the *set* $\mathscr{S}_n$ of 4^n generalised Pauli matrices rather than the group $\mathscr{G}_n$. Doing this, the stabilisers of $\mathscr{G}_n$ transfer to Abelian subsets of $\mathscr{S}_n$, called *pseudo*stabilisers. The largest possible subsets of $\mathscr{S}_n$ whose elements all mutually commute have 2^n elements, and are denoted s_n^a, where a labels the different subsets. These *maximal* pseudostabilisers form the foundation of this discretisation procedure.

Finally, the Hilbertian polytope $\mathfrak{H}_\mathfrak{n}$ is defined as the set of n-qubit state vectors that are the common eigenvectors of the elements of s_n^a, for all subsets a.

The uniform Hilbertian polytope on n qubits $\mathfrak{H}_\mathfrak{n}$ contains

$$V_n = 2^n \prod_{k=0}^{n-1} (2^{n-k} + 1)$$

vertices, or states. The following table gives the first values of V_n, along with C_n, the number of classical bit configurations for comparison.

n	1	2	3	4	5	6	7
V_n	6	60	1080	36720	2423520	315057600	81284860800
C_n	2	4	8	16	32	64	128

V_n grows as $2^{(n^2+3n)/2}$, so the information content is super-extensive in n.

We now turn to an explicit construction of the uniform Hilbertian polytope for the one- and two-qubit cases.

https://doi.org/10.1017/S0960129507006329 Published online by Cambridge University Press

3.2. *The one-qubit case:* $\mathfrak{H}_1$

We show here that $\mathfrak{H}_1$ is isomorphic to an octahedron. For one qubit, the set $\mathscr{S}_n$ is simply the Pauli matrices: $\mathscr{S}_1 = \{\sigma_w, \sigma_x, \sigma_y, \sigma_z\}$. The last three $\sigma's$ anti-commute with one another, while they all commute with the identity σ_w. So the three sets of mutually commuting matrices are trivial to construct: $s_1^1 = \{\sigma_w, \sigma_z\}$, $s_1^2 = \{\sigma_w, \sigma_x\}$ and $s_1^3 = \{\sigma_w, \sigma_y\}$.

When the elements of s_1^l are diagonalised (for $l = 1, 2, 3$), we obtain the following six states, which sit on an octahedron on the Bloch sphere:

$$\begin{aligned} |+z\rangle &= |0\rangle, & |-z\rangle &= |1\rangle \\ |+x\rangle &= \tfrac{1}{\sqrt{2}}\left(|0\rangle + |1\rangle\right), & |-x\rangle &= \tfrac{1}{\sqrt{2}}\left(|0\rangle - |1\rangle\right) \\ |+y\rangle &= \tfrac{1}{\sqrt{2}}\left(|0\rangle + i\,|1\rangle\right), & |-y\rangle &= \tfrac{1}{\sqrt{2}}\left(|0\rangle - i\,|1\rangle\right). \end{aligned}$$

3.3. *The two-qubit case:* $\mathfrak{H}_2$

The set of generalised Pauli matrices for two qubits $\mathscr{S}_2$ comprises 16, 4×4 matrices given by $\Sigma_{\lambda\mu} = \sigma_\lambda \otimes \sigma_\mu$, with $\lambda, \mu = w, x, y, z$.

One finds fifteen pseudostabilisers, yielding four simultaneous eigenvectors each and contributing four states to $\mathfrak{H}_2$. We therefore recover the result that $\mathfrak{H}_2$ has sixty states. These subsets can be classified as corresponding to entangled or product states. Nine sets correspond to product states, and the other six (marked with an *) correspond to maximally entangled states. We list these eigenvectors in Table 1 as unnormalised row vectors.

Note that the first stabiliser of the product sector corresponds to the computational basis, while the first stabiliser of the entangled sector corresponds to the Bell basis.

3.4. *Connection with an alternate approach to discretisation: shelling the high-dimensional dense lattices*

We will now present another, more geometrical, approach to Hilbert space discretisation, which uses the successive shells of dense lattices in $\mathbb{R}^{2^{n+1}}$ to discretise the high dimensional hyperspheres. At the same time, we must take into account the global phase freedom, and show how a discretisation of the projective Hilbert space is induced (this means that several points on S^{2^n-1} will represent the same physical state). In the light of this, it is important to distinguish between 'qubit states' (the quantum states associated with the points on S^{2^n-1}) and 'physical states' (the states in the projective Hilbert space, which has the geometry of a complex projective space CP^{2^n-1}).

We consider the family of laminated lattices Λ_i. These laminated lattices form a series that starts with the triangular lattice in $2d$ (the densest lattice in $2d$). Λ_3 is obtained as a particular sequence of Λ_2 lattices packed in a third dimension, which gives the face-centred cubic lattice, one of the two densest lattices in $3d$. Appropriately packing Λ_3 lattices along a fourth dimension leads to Λ_4, whose first shell is precisely the $\{3, 4, 3\}$ polytope (Coxeter 1973), which we will use here for the one-qubit case. Upon iteration, this construction eventually leads to the $\Lambda_8 = E_8$ lattice suitable for the two-qubit case.

https://doi.org/10.1017/S0960129507006329 Published online by Cambridge University Press

Table 1.

Set				
1	$(0,0,0,1)$	$(0,1,0,0)$	$(0,0,1,0)$	$(1,0,0,0)$
2	$(0,0,-1,1)$	$(-1,1,0,0)$	$(0,0,1,1)$	$(1,1,0,0)$
3	$(0,0,i,1)$	$(i,1,0,0)$	$(0,0,-i,1)$	$(-i,1,0,0)$
4	$(0,-1,0,1)$	$(0,1,0,1)$	$(-1,0,1,0)$	$(1,0,1,0)$
5	$(1,-1,-1,1)$	$(-1,1,-1,1)$	$(-1,-1,1,1)$	$(1,1,1,1)$
6	$(-i,-1,i,1)$	$(i,1,i,1)$	$(i,-1,-i,1)$	$(-i,1,-i,1)$
7	$(0,i,0,1)$	$(0,-i,0,1)$	$(i,0,1,0)$	$(-i,0,1,0)$
8	$(-i,i,-1,1)$	$(i,-i,-1,1)$	$(i,i,1,1)$	$(-i,-i,1,1)$
9	$(-1,i,i,1)$	$(1,-i,i,1)$	$(1,i,-i,1)$	$(1,i,i,-1)$
10*	$(0,-1,1,0)$	$(-1,0,0,1)$	$(1,0,0,1)$	$(0,1,1,0)$
11*	$(i,0,0,1)$	$(0,-i,1,0)$	$(0,i,1,0)$	$(-i,0,0,1)$
12*	$(1,1,-1,1)$	$(-1,1,1,1)$	$(1,-1,1,1)$	$(1,1,1,-1)$
13*	$(i,-i,1,1)$	$(i,i,-1,1)$	$(i,i,1,-1)$	$(-i,i,1,1)$
14*	$(i,1,-i,1)$	$(-i,1,i,1)$	$(i,-1,i,1)$	$(i,1,i,-1)$
15*	$(-1,-i,i,1)$	$(-1,i,-i,1)$	$(1,-i,-i,1)$	$(1,i,i,1)$

We shall focus here on the set of 240 sites belonging to the E_8 first shell that forms the so-called *Gosset polytope* and, as for the one-qubit case, enumerate the physical states they represent. Finally, we will present new results with a set of 1080 discrete 3-qubits states that originate from the 16-dimensional dense lattice Λ_{16}.

3.5. *The one-qubit case and the* Λ_4 *lattice*

We give two possible (dual) coordinates for the $\{3,4,3\}$ vertices: in each case as a real quadruplet and a complex pair. The correspondence between real quadruplets and complex pairs amounts simply to taking the first two (last two) real numbers as the real and imaginary part of the first (second) complex number. The first (second) complex number in the pair corresponds to t_0 (t_1).

A first set, denoted T_1, is the union of the eight permutations of type $(\pm 1,0,0,0)$ and the sixteen permutations of type $\frac{1}{2}(\pm 1,\pm 1,\pm 1,\pm 1)$. Note that, modulo a global phase factor, these twenty-four points really represent six different physical states, which appear on the Bloch sphere as opposite points on the three orthogonal axes x,y,z. Indeed, the

https://doi.org/10.1017/S0960129507006329 Published online by Cambridge University Press

four points given in the following table

Real quadruplets	Complex pairs
$(1,0,0,0)$	$(1,0)$
$(-1,0,0,0)$	$(-1,0)$
$(0,1,0,0)$	$(i,0)$
$(0,-1,0,0)$	$(-i,0)$

represent the states $|\Psi_1,\omega\rangle = e^{i\omega}|0\rangle$, with $\omega = 0,\pi/2,\pi,3\pi/2$, which map to the same point on the Bloch sphere (the north pole), and they are therefore associated with the physical state $|\Psi_1\rangle$. Equivalently, the four points given in the following table

Real quadruplets	Complex pairs
$(0,0,1,0)$	$(0,1)$
$(0,0,-1,0)$	$(0,-1)$
$(0,0,0,1)$	$(0,i)$
$(0,0,0,-1)$	$(0,-i)$

represent the four states $|\Psi_2,\omega\rangle = e^{i\omega}|1\rangle$ with $\omega = 0,\pi/2,\pi,3\pi/2$. The other sixteen vertices represent four other physical states as follows:

$$|\Psi_3\rangle \equiv \frac{e^{i(\omega+\pi/4)}}{\sqrt{2}}\left(|0\rangle - |1\rangle\right), \qquad |\Psi_4\rangle \equiv \frac{e^{i(\omega+\pi/4)}}{\sqrt{2}}\left(|0\rangle - |1\rangle\right),$$
$$|\Psi_5\rangle \equiv \frac{e^{i(\omega+\pi/4)}}{\sqrt{2}}\left(|0\rangle + i|1\rangle\right), \qquad |\Psi_6\rangle \equiv \frac{e^{i(\omega+\pi/4)}}{\sqrt{2}}\left(|0\rangle - i|1\rangle\right),$$

with $\omega = 0,\pi/2,\pi,3\pi/2$.

It will be useful for the discrete two-qubit construction given later to describe a second version of the polytope $\{3,4,3\}$, in which the twenty-four vertices form a set T_2 given by twenty-four permutations of the type $\{\pm 1,\pm 1,0,0\}/\sqrt{2}$. This polytope is obtained from the original one by means of a *screw* motion on S^3 of angle $\pi/4$. This set leads to twenty-four states

$$|\Phi_l,\omega\rangle = \epsilon\,|\Psi_l,\omega\rangle, \quad l = 1..6, \quad \omega = 0,\pi/2,\pi,3\pi/2, \text{ and } \quad \epsilon = e^{i\pi/4}$$

and to the six one-qubit physical states $|\Phi_l\rangle$ identical to $|\Psi_l\rangle$. Indeed, the six states $|\Psi_j\rangle$ sit at the vertices of a regular octahedron. Since the only difference between the states $|\Phi_l,\omega\rangle$ and $|\Psi_l,\omega\rangle$ is a global phase, they map onto the same six points on the Bloch sphere.

3.6. *The two-qubit case and the E_8 lattice*

The 240 vertices of the Gosset polytope belong to a sphere S^7. These 240 vertices may be separated into ten equivalent subsets, each belonging to non-intersecting S^3 spheres. This

https://doi.org/10.1017/S0960129507006329 Published online by Cambridge University Press

is just a discrete version of the S^7 Hopf fibration, with fibers S^3 and base S^4(Sadoc and Mosseri 1999; Sadoc and Mosseri 1993; Manton 1987).

We use here quaternionic coordinates instead of complex or real ones. The above set T_1, scaled such that the corresponding points belong to a sphere S^3 of radius $\frac{1}{\sqrt{2}}$, is now given by

$$T_1 = \{\pm\frac{1}{\sqrt{2}}, \pm\frac{\mathbf{i}}{\sqrt{2}}, \pm\frac{\mathbf{j}}{\sqrt{2}}, \pm\frac{\mathbf{k}}{\sqrt{2}}, \frac{1}{2\sqrt{2}}(\pm 1 \pm \mathbf{i} \pm \mathbf{j} \pm \mathbf{k})\},$$

where $\mathbf{i}, \mathbf{j}$ and $\mathbf{k}$ are the standard unit quaternions. The set T_2 stays on a unit sphere and is given by

$$T_2 = \{\frac{1}{\sqrt{2}}(\pm 1 \pm \mathbf{i}), \frac{1}{\sqrt{2}}(\pm 1 \pm \mathbf{j}), \frac{1}{\sqrt{2}}(\pm 1 \pm \mathbf{k}), \frac{1}{\sqrt{2}}(\pm \mathbf{i} \pm \mathbf{j}), \frac{1}{\sqrt{2}}(\pm \mathbf{i} \pm \mathbf{k}), \frac{1}{\sqrt{2}}(\pm \mathbf{j} \pm \mathbf{k})\}.$$

The 240 vertices of the Gosset polytope belong to the ten sets:

$$S_1 = (T_2, 0), \quad S_2 = (0, T_2), \quad S_3 = (T_1, T_1), \quad S_4 = (T_1, -T_1),$$
$$S_5 = (T_1, \mathbf{i}T_1), \quad S_6 = (T_1, -\mathbf{i}T_1), \quad S_7 = (T_1, \mathbf{j}T_1), \quad S_8 = (T_1, -\mathbf{j}T_1),$$
$$S_9 = (T_1, \mathbf{k}T_1), \quad S_{10} = (T_1, -\mathbf{k}T_1).$$

Each of the ten sets gives a copy of a $\{3, 4, 3\}$ polytope on a fiber S^3. The points can be Hopf mapped, as described above, onto the base space S^4. The location of the mapped point is intimately related to the entanglement of the corresponding two-qubit state.

It is then easy to verify that the sets S_1 to S_6 correspond to separable states, while sets S_7 to S_{10} correspond to maximally entangled states.

More precisely, the six sets $S_1 \cdots S_6$ encompass $6 \times 24 = 144$ vertices, forming 36 physical states in all, with four values of the global phase for each qubit state. Note that the precise value of the phases are important here in order that our discretisation procedure uniformly covers the full Hilbert space. Using the above defined eigenstates of the one-qubit Pauli matrices, these states are given by the following table:

$\|\pm x\rangle \otimes \|\pm x\rangle\, e^{i(\pi/4+m\pi/2)}$	$\|\pm x\rangle \otimes \|\pm y\rangle\, e^{i(\pi/4+m\pi/2)}$	$\|\pm x\rangle \otimes \|\pm z\rangle\, e^{im\pi/2}$
$\|\pm y\rangle \otimes \|\pm x\rangle\, e^{i(\pi/4+m\pi/2)}$	$\|\pm y\rangle \otimes \|\pm y\rangle\, e^{i(\pi/4+m\pi/2)}$	$\|\pm y\rangle \otimes \|\pm z\rangle\, e^{im\pi/2}$
$\|\pm z\rangle \otimes \|\pm x\rangle\, e^{im\pi/2}$	$\|\pm z\rangle \otimes \|\pm y\rangle\, e^{im\pi/2}$	$\|\pm z\rangle \otimes \|\pm z\rangle\, e^{i(\pi/4+m\pi/2)}$

where $m = 0, 1, 2, 3$ triggers the global phase. Each of the nine entries stands for the four possible sign combinations, leading to the thirty-six physical states mentioned earlier. A simple view of these separable states consists in relating them to the 'product' of two octahedra, each one belonging to the Bloch sphere of the individual qubits.

The remaining four sets ($4 \times 24 = 96$ sites in all) lead to a slightly more subtle structure. We find a total of twenty-four different physical MES, with four phase-distinct two-qubit states for each. But in the present case, the phase-distinct states actually belong to two different sets, either (S_7, S_8) or (S_9, S_{10}). These twenty-four physical states can be written

https://doi.org/10.1017/S0960129507006329 Published online by Cambridge University Press

as in the following table:

$\frac{1}{\sqrt{2}}\left(\|+z,+z\rangle + e^{i\theta}\|-z,-z\rangle\right)$	$\frac{1}{\sqrt{2}}\left(\|+z,-z\rangle + e^{i\theta}\|-z,z\rangle\right)$
$\frac{1}{\sqrt{2}}\left(\|+z,+x\rangle + e^{i\theta}\|-z,-x\rangle\right)$	$\frac{1}{\sqrt{2}}\left(\|+z,-x\rangle + e^{i\theta}\|-z,+x\rangle\right)$
$\frac{1}{\sqrt{2}}\left(\|+z,+y\rangle + e^{i\theta}\|-z,-y\rangle\right)$	$\frac{1}{\sqrt{2}}\left(\|+z,-y\rangle + e^{i\theta}\|-z,+y\rangle\right)$

with $\theta = 0, \pi/2, \pi, 3\pi/2$.

Note that these twenty-four entangled states, together with the above thirty-six separable states, are in one-to-one correspondence, up to a global phase, with the sixty discrete states on $\mathfrak{H}_2$ presented earlier.

3.7. *Finer discretisations of H_2: higher E_8 shells*

The present lattice approach has the benefit of allowing finer discrete sets to be explored in a straightforward manner by considering the higher-order shells in E_8. This construction would provide a uniform set of two-qubit states, some of which would have intermediate entanglement. A note of caution is in order here, since we are only interested in describing normalised quantum states. Lattice points that are aligned, as viewed from the origin, contribute to the same two-qubit state.

We will not give here a detailed description of these finer discretisations of H_2. However, we note that the number M_J of sites on the J^{th} shell around an E_8 vertex is simply given by

$$M_J = 240 \sum_{d|J} d^3,$$

where d denotes integers that divide J (Conway and Sloane 1988). The table below displays these numbers for the first four shells.

J	1	2	3	4
M	240	2160	6720	17520

Again, the physical states are obtained from these two-qubit states by modding out a global phase.

The shell-by-shell analysis, and its relation to the Hopf map, has been given elsewhere (Sadoc and Mosseri 1999; Sadoc and Mosseri 1993). It allows us to get points on the second shell corresponding to states having concurrence $0, 1/2, 1/\sqrt{2}, 1$. The third shell contributes states of concurrence 0, 1/3, 2/3, $\sqrt{5}/3$, $\sqrt{8}/3$ and 1.

3.8. *The three-qubit case: $\mathfrak{H}_3$ and the Λ_{16} lattice*

This case should be related to the dense lattice Λ_{16} in $\mathbb{R}^{16}$ (Conway and Sloane 1988). It is interesting to note that the number of lattice sites closest to the origin – the lattice 'kissing number' – for this case is 4320, which is precisely four times the expected number of vertices on the uniform Hilbertian polytope $\mathfrak{H}_3$. We are therefore likely to face a similar

https://doi.org/10.1017/S0960129507006329 Published online by Cambridge University Press

situation to the one we faced with the one- and two-qubit cases, where there were four phase-related qubit states associated with each physical state. And, indeed, the four-to-one relation between the Λ_{16} first shell sites and the vertices of $\mathfrak{H}_3$ has been checked.

With a suitably oriented S^{15} Hopf fibration, the 4320 sites in the first shell can be organised as 18 sets of 240 sites belonging to an S^7 fibre; each such set is a copy of a 240-site Gosset polytope, which therefore shows a nice nested structure. The 18 sets are uniquely defined by the coordinates of the corresponding point on the base space S^8. The corresponding 18-site polytope is just the 'cross polytope' in $\mathbb{R}^9$, with two opposite points along 9 orthogonal directions.

Upon modding out the global phase, we find that, as with the entangled 2-qubit states, some phase-distinct states belong to different fibres. The 1080 discrete 3-qubit states belong to three different classes: fully separable, products of one-qubit states and a maximally 2-qubits entangled state, and maximally entangled (as measured by the 3-tangle).

More precisely, among the 18 fibres:

— Six fibres (whose octonionic coordinates on the base space reduce to a complex number) contain states that are either triple product states, or the product of the first qubit and a MES in the remaining two qubits
— The remaining 12 fibres contain states that are either the product of the second or third qubit and a MES in the remaining two qubits, or states with true (and maximal) 3-qubit entanglement, characterised by a 3-tangle equal to unity

As a whole, one gets:

— a set of 216 triple product states;
— a set of 432 states that are the product of one qubit and a MES in the remaining two;
— a set of 432 maximally entangled 3-qubit states (with unit 3-tangle).

Note that the first two sets could have been generated from the two- and one-qubit analysis, with (suitably oriented) Λ_8 and Λ_4, while the third is really new.

The generalisation to more than three qubits cannot use the Hopf fibrations limited to S^{15}. A particularly interesting family to be checked further is the one described long ago by John Leech (Leech 1964), which coincides with those studied here for $N = 1, 2$ and 3, and whose kissing number is, for any N, precisely four times that given in the first part of this paper for the number of states in the generic Hilbertian polytopes.

Acknowledgements

It is a pleasure thank Chad Rigetti and Michel Devoret for the collaboration recalled in the second part of this paper. The only new calculation with respect to what has already been published with them concerns the analysis of the 1080 discrete 3-qubits states.

Pedro Ribeiro was partially supported by FCT and EU FEDER through POCTI and POCI, namely via Quant- Log POCI/MAT/55796/2004 Project of CLC-DM-IST, SQIG-IT and grant SFRH/BD/16182/2004/2ZB5.

References

Bernevig, B. A. and Chen, H.-D. (2003) *J. Phys. A* **36** 8325.

Bouwmeester, D., Eckert, A. and Zeilinger, A. (2000) *The Physics of Quantum Information*, Springer-Verlag.
Coffman, V., Kundu, J. and Wootters, W. (2000) *Phys. Rev. A* **61** 52306.
Conway, J. H. and Sloane, N. J. A. (1988) *Sphere Packings, Lattices and Groups*, Springer-Verlag.
Coxeter, H. S. M. (1973) *Regular Polytopes*, Dover.
Kempe, J. (1999) *Phys. Rev. A* **60** 910.
Kus, M. and Zyczkowski, K. (2001) *Phys. Rev A*. **63** 032307.
Leech, J. (1964) *Canad. J. Math.* **16** 657–682.
Levay, P. (2004) *J. Phys. A* **37** 1821–1842.
Manton, N. S. (1987) *Comm. Math. Phys.* **113** 341–351.
Mosseri, R. (2000) Two-qubit and Three-qubit Geometry and Hopf Fibrations. In: Monastyrsky, M. I. (ed.) Topology in Condensed Matter. *Springer Series in Solid-State Physics* **150** 187–203. (Also available at quant-ph/0310053.)
Mosseri, R. and Dandoloff, R. (2001) *J. Phys. A* **34** 10243–10252.
Nielsen, M. A. and Chuang, I. L. (2000) *Quantum Information and Quantum Computation*, Cambridge University Press.
Rigetti, C., Mosseri, R. and Devoret, M. (2004) Geometric Approach to Digital Quantum Information. *Quantum Information Processing* **3** (6) 351–380. (Also available at quant-ph/0312196.)
Sadoc, J. F. and Mosseri, R. (1993) *J. Phys. A* **26** 1789–189.
Sadoc, J. F. and Mosseri, R. (1999) *Geometric Frustration*, Cambridge University Press.
Urbanke, H. (1991) *American Journal of Physics* **59** 53.
Wootters, W. K. (1998) *Phys. Rev. Lett.* **80** 2245.